01 Jun 2021

# Mechanical Properties, Translucency, And Low Temperature Degradation (LTD) Of Yttria (3–6 Mol%) Stabilized Zirconia

R. Sharon Uwanyuze
*Missouri University of Science and Technology*, ruvhg@mst.edu

Sulekha Ramesh

Mark K. King

Nathaniel Lawson

*et. al. For a complete list of authors, see https://scholarsmine.mst.edu/matsci_eng_facwork/3255*



## Recommended Citation

R. S. Uwanyuze et al., "Mechanical Properties, Translucency, And Low Temperature Degradation (LTD) Of Yttria (3–6 Mol%) Stabilized Zirconia," *Ceramics International*, vol. 47, no. 11, pp. 15868 - 15874, Elsevier, Jun 2021.
The definitive version is available at https://doi.org/10.1016/j.ceramint.2021.02.161

Ceramics International 47 (2021) 15868–15874

Contents lists available at ScienceDirect

Ceramics International

journal homepage: www.elsevier.com/locate/ceramint

# Mechanical properties, translucency, and low temperature degradation (LTD) of yttria (3–6 mol%) stabilized zirconia

R. Sharon Uwanyuze [a,1], Sulekha Ramesh [a,b], Mark K. King Jr. [a,2], Nathaniel Lawson [c], Manoj K. Mahapatra [a,*]

[a] Department of Materials Science and Engineering, University of Alabama at Birmingham, Birmingham, AL, USA
[b] Bob Jones High School, Madison, AL, USA
[c] School of Dentistry, University of Alabama at Birmingham, Birmingham, AL, USA

ARTICLE INFO

*Keywords:*
$Y_2O_3$–$ZrO_2$
Hardness
Strength
Optical properties
Low temperature degradation

ABSTRACT

The mechanical properties (hardness and biaxial flexural strength), optical properties (translucency and gloss), and low temperature degradation (LTD) of 3–6 mol% yttria stabilized zirconia have been investigated. The specimens were prepared by conventional solid-state sintering at 1400 °C. The mechanical and optical properties were evaluated for sintered and polished specimens. X-ray diffractometer (XRD) and scanning electron microscope (SEM) were used, respectively, for structural and microstructural investigation. LTD was determined by XRD analysis of the samples aged in a hydrothermal autoclave at 134 °C for 5–108 h. The mechanical and optical properties are found to be microstructure sensitive. The LTD, due to tetragonal to monoclinic phase transformation, decreases with increasing $Y_2O_3$ content. The mechanical strength, translucency, and LTD are the lowest for 6 mol% $Y_2O_3$ stabilized zirconia.

## 1. Introduction

The market share of zirconia as metal-free dental restoratives continues to grow along with titanium in the global dental implant market [1]. In addition to the comparable performance with titanium, zirconia exhibits superior aesthetic in relevance to tooth [2–4]. 3 mol% $Y_2O_3$ stabilized tetragonal zirconia (3YZ) has been extensively investigated for dental restorations. However, premature failure of zirconia femoral heads and subsequent recall of hip implants by the manufacturers in 2001 [5] triggers concern for the premature failure of zirconia dental prosthesis. In vivo tetragonal to monoclinic phase ($t \rightarrow m$) transformation of zirconia - aging/low temperature degradation (LTD) and microstructural defects contributed to femoral head fracture [6–8]. LTD of 3YZ of various brands causes surface uplift/roughening and microcrack formation to release the stress due to $t \rightarrow m$ transformation accompanied with volume expansion [9–11]. LTD also degrades the mechanical strength, hardness, fracture toughness [12], and translucency [13] of 3YZ.

Water adsorption and incorporation into the oxygen vacancies in 3YZ and subsequent annihilation of oxygen vacancies promotes $t \rightarrow m$ transformation [14–18]. Chemical homogeneity and grain sizes in YZ microstructure, dictated by sintering conditions, also influence LTD [19]. One study shows that sintering of 3YZ at 1550 °C results in $Y^{3+}$ enrichment in some grains, which transformed into cubic phase, followed by surrounding $Y^{3+}$ depleted tetragonal grains - the nucleation sites for LTD [20]. The $t \rightarrow m$ transformation decreases from 6.64% to 2.54% after aging for 5 h at 134 °C at 2 bar as the grain size of yttria stabilized tetragonal zirconia decreases from 0.574 μm to 0.372 μm [21]. Another study reports that the LTD increases at 170 °C and 200 °C with decreasing particle size from 0.77 μm to 0.69 μm of tetragonal YZ powders [18]. The apparent anomaly may be attributed to the powder characteristics such as powder composition and morphology as well as the microstructure of the sintered product. Nonetheless, grain size in the sintered YZ definitely impacts $t \rightarrow m$ transformation to maintain thermodynamic stability [22]. A phase stability diagram of zirconia, based on surface energetics, reveals that the tetragonal and cubic polymorphs would be stable for the crystal sizes smaller than 53 nm and 6 nm, respectively [23]. This study is consistent with $Y_2O_3$–$ZrO_2$ phase

* Corresponding author.
*E-mail address:* mkmanoj@uab.edu (M.K. Mahapatra).
[1] Present affiliation: Department of Materials Science and Engineering, University of Connecticut, Storrs, Connecticut.
[2] Present affiliation: Moog Inc. Blacksburg, Virginia.

https://doi.org/10.1016/j.ceramint.2021.02.161
Received 29 November 2020; Received in revised form 1 February 2021; Accepted 18 February 2021
Available online 21 February 2021

diagrams [24,25] which conclude that the tetragonality of zirconia decreases with increasing $Y_2O_3$ content.

The strategies considered to minimize LTD, if not completely eliminated, include doping YZ with different oxides [19,26–29], decreasing grain size by controlled sintering [19,30], and decreasing the tetragonality of YZ [12,31–33]. $Al_2O_3$, $La_2O_3$, and $SiO_2$ are commonly studied dopants. The dopants segregate at the grain boundaries to reduce its energy and generate more oxygen vacancies (except for $SiO_2$) to maintain charge neutrality. The cations at the grain boundaries electrostatically couple with the oxygen vacancies. Consequently, the LTD decelerates. However, above a critical concentration the dopants segregate at the grains and favors LTD. For instance, 0.25 wt% $Al_2O_3$ retards LTD but higher concentrations do not [28]. In fact, an $Al_2O_3$ doped new generation zirconia accelerated LTD in vivo, perhaps due to its concentration above the critical value [34]. The dopants, depending on the ionic size, induce partial transformation of tetragonal phase into the cubic phase.

It has been shown that the abundance of oxygen vacancies and their distribution makes cubic YZ more stable than the tetragonal phase [35]. The higher stability perhaps decelerates the LTD of cubic YZ [12,31]. Demonstration of cubic YZ degradation at 250 °C [14] infers that it is not actually LTD proof but slow kinetics. Crystallographic symmetry also improves the translucency of cubic phase [32]. However, tetragonal phase is preferred for its superior mechanical strength and excessive oxygen vacancies in YZ favors LTD [36]. Therefore, a trade-of between LTD, mechanical properties, and translucency is desired, which may be achieved by simultaneous presence of cubic and tetragonal phase with optimized microstructure free of pores and cracks, and secondary phase segregation at the grains.

It is noteworthy that most of the LTD reports in literature are based on the commercial manufacturers of zirconia prosthesis. The exact composition and processing parameters are proprietary, which may lead to difficulties in decoupling the different aspects on the fundamental composition-structure-property relationship. 3–6 mol% $Y_2O_3$ stabilized zirconia has been investigated in the present study to understand the compositional effect on LTD, mechanical properties, and translucency. More than 3 mol% $Y_2O_3$ generates mixed cubic and tetragonal phase according to phase diagram [25] while absence of other dopants eliminates secondary phase segregation and these compositions are unlikely to generate excess oxygen vacancies.

## 2. Materials and methods

### 2.1. Sample preparation

4–6 mol% yttria stabilized zirconia (YSZ) was prepared by mixing appropriate amounts of 3 mol% (3YB-E) and 8 mol% (TZ-8YS) $Y_2O_3$ stabilized zirconia powders (Tosoh-zirconia, Japan) by dry-mixing for overnight in a ball mill using zirconia ball. The powders were uniaxially pressed at 335 MPa into 13 mm diameter and ~2 mm thick cylindrical pellets. The pellets were sintered (pressureless) at 1300–1500 °C in air for 5 h dwell time at 5 °C/min ramp rate during heating and cooling as well. The sintered pellets were identified as 3YZ, 4YZ, 5YZ, and 6YZ, respectively, for 3 mol%, 4 mol%, 5 mol%, and 6 mol% $Y_2O_3$ content in the batch composition.

### 2.2. Evaluation of properties

#### 2.2.1. Bulk density and apparent porosity

Bulk density and apparent porosity of the sintered samples were determined by Archimedes principle, according to ASTM C373-88 [37]. At least five samples were used and the average values are reported. The samples sintered at 1400 °C were used for further characterizations.

#### 2.2.2. Mechanical properties

Biaxial flexural strength of the sintered samples were evaluated according to ISO 6872:2015 [38]. The specimens were supported by three hardened steel balls (4.5 ± 0.2 mm diameter) positioned 120° apart in the fixture in a universal testing machine. The load was applied with a flat punch with a diameter of (1.4 ± 0.2) mm at the center of the specimen with 1 mm/min crosshead speed. The biaxial flexural strength ($\sigma$) is calculated by:

$$\sigma = \frac{-0.2387P(X-Y)}{b^2}$$

Where P = load causing failure (N),

$$X = (1+\vartheta)\ln\left(\frac{r_2}{r_3}\right)^2 + \left[\frac{(1-\vartheta)}{2}\right]\left(\frac{r_2}{r_3}\right)^2$$

$$Y = (1+\vartheta)\left[1+ln\left(\frac{r_1}{r_3}\right)^2\right] + (1-\vartheta)\left(\frac{r_1}{r_3}\right)^2$$

b = specimen thickness, mm
$\vartheta$ = *Poisson's ratio*, 0.3
$r_1$ = radius of support circle, mm
$r_2$ = radius of loaded area, mm
$r_3$ = radius of speciemn, mm

Top and bottom surfaces of the sintered samples were manually polished to an optical finish sequentially with 30 μm, 15 μm, 9 μm, 3 μm, and 1 μm diamond paste. Manual polishing was performed to avoid stress induced *t→m* transformation at the surface. The polished samples were divided into four groups.

One group of the polished samples were used for hardness measurement by Vicker's indentation method (ASTM C1327 – 15) [39] using 1 kg load (Micromet II, Buehler, IL, USA). At least 10 indents were used. The Vickers hardness (GPa) was computed as

$$HV\ (GPa) = 0.0018544\left(\frac{P}{d^2}\right)$$

Where, P = force (N) and d = average length of the two diagonals of the indentation, mm.

#### 2.2.3. Optical properties

One group of the polished samples were used for translucency and glossiness measurement. The translucency parameter was determined by modified CIELAB equation [40]. The CIE L*a*b* parameters were measured on white and black backgrounds using a Munsell-like neutral value scale sheet background with a spectrophotometer (Color-i7, X-Rite, Grand Rapids, MI, USA), in reflectance mode, and using CIE L*a*b* system. The spectrophotometer was calibrated according to the manufacturer's instructions before each reading. The specimens were placed in direct contact with the aperture and no coupling medium was applied. The reading was repeated three times for each specimen and the average value was used for the analysis. Translucency parameter was measured as the difference in L*a*b* read on white and black backgrounds. Translucency parameter, $\Delta E_{2000}$, was calculated by the equation below:

$$\Delta E_{2000} = \left[\left(\frac{\Delta L'}{K_L S_L}\right)^2 + \left(\frac{\Delta C'}{K_c S_C}\right)^2 + \left(\frac{\Delta H'}{K_H S_H}\right)^2 + R_T\left(\frac{\Delta C'}{K_C S_c}\right)\left(\frac{\Delta H'}{K_H S_H}\right)\right]^{1/2}$$

where ΔL', ΔC', and ΔH' are differences in lightness, chroma, and hue; $R_T$ (rotation function) accounts for the interaction between hue and chroma in the blue region; $S_L$, $S_C$, and $S_H$ adjust for variation in the L*a*b* coordinate system; and $K_L$, $K_C$, and $K_H$ correct for experimental conditions ($K_L = 1.0$, $K_C = 1.0$, $K_H = 1.0$ for this study).

Gloss of the polished samples were measured using a glossmeter (Novo-curve Small Area Glossmeter, UK) using 60° geometry. At least

ten gloss unit (GU) values from each specimen was recorded and averaged.

#### 2.2.4. Low temperature degradation

The low temperature degradation (LTD) of the specimens was evaluated by accelerated artificial hydrothermal aging at 134 °C in a Teflon vessel enclosed in a high pressure container. The *t→m* transformation was identified by X-ray diffraction technique in 27–35° 2Θ range. The amount of monoclinic phase was quantified according to Ref. [41].

$$X_m = \frac{I^m_{(111)} + I_{(\bar{1}11)}{}^m}{I^m_{(111)} + I_{(\bar{1}11)}{}^m + I^t_{(101)}}$$

where, $X_m$ is the fraction of monoclinic phase; $I^m$ and $I^t$ are the intensities, respectively, for the monoclinic phase and tetragonal phases. The subscripts in $I^m$ and $I^t$ indicate the corresponding crystallographic planes.

#### 2.2.5. Structural and microstructural characterizations

The crystal structure of the sintered specimens and the LTD specimens were identified by X-ray diffraction technique (Siemens D500, KRISTALLOFLEX DACO-MP 710/710 H) using Cu $K_\alpha$ radiation ($\lambda$ = 1.5406 Å). The sintered samples and the LTD specimens were scanned, respectively, in 20°–80° and 27°–35° 2Θ range with 0.03° step size and 30 s dwell/step. The crystal structure was identified using Jade 10 analysis software and International Centre for Diffraction Data (ICDD).

Scanning electron microscope (SEM) (SEM, FEI Quantity 650 FEG) was used to characterize the microstructure of the polished and thermally etched (1300 °C for 30 min) sintered samples. Energy dispersive spectrometer (EDS, AMETEK EDAX) attached to the SEM was used for the elemental compositional analysis and reported in atomic%.

## 3. Results and discussion

### 3.1. Density and porosity

Bulk densities and apparent porosities of the YZ specimens sintered at 1300–1500 °C range are shown in Table 1. The highest densities of 3YZ and 4YZ are found at 1400 °C sintering temperature but 1500 °C for 5YZ and 1300 °C for 6YZ specimens. The density decreases with increasing $Y_2O_3$ content because of its lower structural density than that of $ZrO_2$. No specific trend in density has been observed with either $Y_2O_3$ content or temperature. However, the specimens sintered at 1400 °C were selected for evaluation of different properties. The apparent porosity follows the opposite trend, as obvious, compared to the density.

### 3.2. Crystal structure and microstructure

The XRD plots of the sintered YZ specimens are shown in Fig. 1. The Bragg's diffraction angle for the crystallographic planes of the tetragonal and cubic polymorphs are too close to discern. The peak splitting corresponding to the tetragonal polymorph in 3YZ, however, decreases with increase in $Y_2O_3$ content and tend to disappear for 6YZ. This observation qualitatively confirms that the fraction of cubic polymorph increases with more than 3 mol% $Y_2O_3$ content, consistent with the $Y_2O_3$–$ZrO_2$ phase diagram [25].

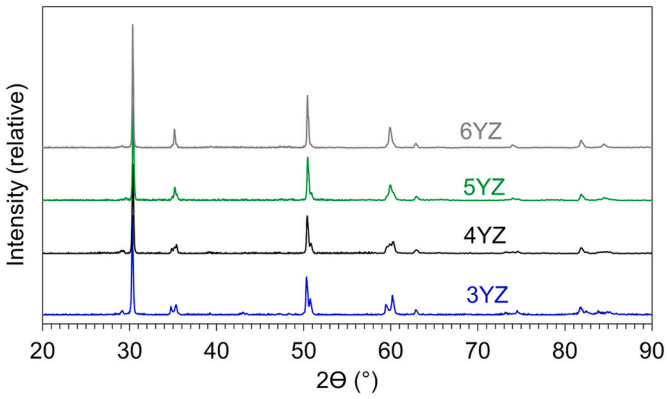


**Fig. 1.** XRD plots YZ samples sintered at 1400 °C for 5 h.

The SEM images of the sintered specimens are shown in Fig. 2. The grain sizes are determined by linear intercept method. 0.33 ± 0.03 μm grains along with few larger grains are observed in the 3YZ. 0.32 ± 0.02 μm grains are observed in 4YZ. Large (2.04 ± 0.38 μm) and small (0.34 ± 0.04 μm) grains are localized in 5YZ. Similarly, larger grains (2.20 ± 0.46 μm) are mostly surrounded by the smaller grains (0.30 ± 0.02 μm) in 6YZ. Smaller grains in 6YZ are also localized but apparently to the lower extent than 5YZ. Higher $\frac{Y}{Zr}$ ratio has been found for the larger grains than the smaller grains for all the studied specimens - a general trend as shown in Table 2. The difference in the diffusivity of $Y^{3+}$ ions and $O^{2-}$ ions $\left(D_{O^{2-}} > D_{Y^{3+}}\right)$ [42] plausibly attributes to the varying $\frac{Y}{Zr}$ ratio. Sporadic pores are present in all the specimens with a negligible extent for 3YZ. The increased amount of pores in the microstructure of the remaining specimens is consistent with the measured apparent porosity. Pores are present at the grain boundaries as well as inside the grains of 5YZ and 6YZ specimens (Fig. 2d–f) while only at the grain boundaries in a localized region of 4YZ (Fig. 2b).

### 3.3. Mechanical properties

The fracture strengths of the YZ specimens sintered at 1400 °C are shown in Fig. 3. The fracture strength of 3YZ is comparable with a recent study [43]. The fracture strength decreases with increase in $Y_2O_3$ content, which may be attributed to the pores - the defects to originate fracture. Pores are agglomerated in local region of 4YZ (Fig. 2b), and are sporadically distributed at the grains and grain boundaries of 5YZ and 6YZ. The pores are the stress concentrator for mechanical failure. In addition, microstructural heterogeneity (large and small grain sizes at selected regions, and compositional variation) causes non-uniform stress distribution under uniaxial load, causing strength decrease [44]. However, the average values of fracture strengths are comparable, except for 6YZ, considering the standard deviation. It is noted that the standard deviation increases with $Y_2O_3$ content, likely due to higher porosity and its non-uniform distribution.

The microhardness values, obtained by Vickers indentation method, of the YZ specimens in Fig. 4 do not change significantly with increase in $Y_2O_3$ content. Slight increase in hardness for 6YZ is within the experimental error limit as reflected in the error bar. The hardness value of

**Table 1**
Bulk density and apparent porosity of 3–6 mol% Y2O3 stabilized zirconia sintered at 1300–1500 °C for 5 h.

| Sample | 1300 °C | | 1400 °C | | 1500 °C | |
|---|---|---|---|---|---|---|
| | Density (g/cm$^3$) | Apparent porosity (%) | Density (g/cm$^3$) | Apparent porosity (%) | Density (g/cm$^3$) | Apparent porosity (%) |
| 3YZ | 5.96 ± 0.11 | 1.41 ± 1.0 | 6.07 ± 0.07 | 0.42 ± 0.34 | 5.98 ± 0.02 | 0.72 ± 0.27 |
| 4YZ | 5.85 ± 0.05 | 1.6 ± 0.97 | 5.98 ± 0.04 | 0.82 ± 0.75 | 5.96 ± 0.03 | 0.79 ± 0.47 |
| 5YZ | 5.79 ± 0.04 | 1.51 ± 0.39 | 5.87 ± 0.02 | 2.57 ± 0.25 | 5.93 ± 0.03 | 1.15 ± 0.52 |
| 6YZ | 5.82 ± 0.05 | 1.44 ± 0.68 | 5.72 ± 0.06 | 4.04 ± 1.25 | 5.78 ± 0.05 | 2.86 ± 0.74 |

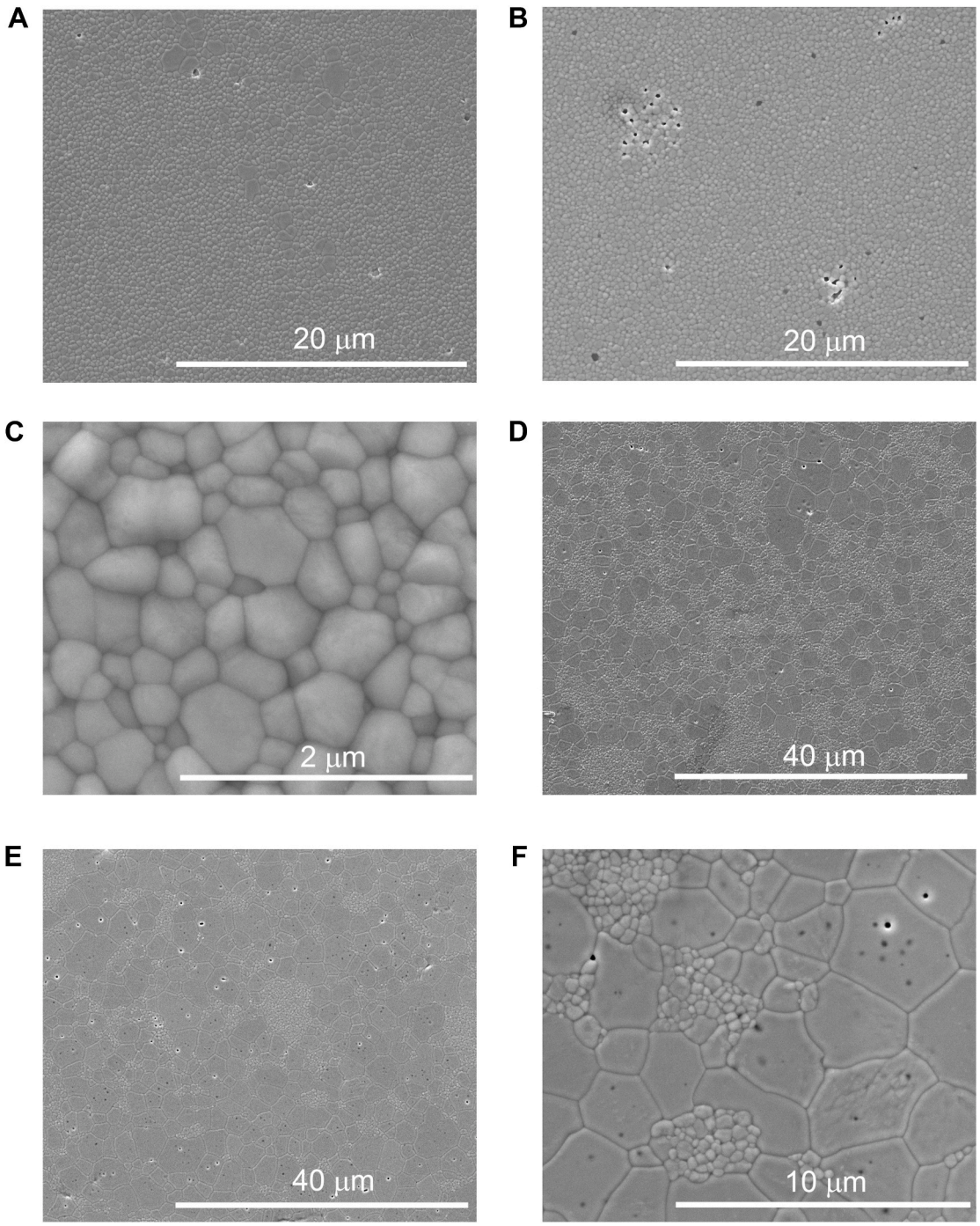


**Fig. 2.** SEM images of YZ samples sintered at1400 °C for 5 h: (a) 3YZ, (b) 4YZ at low magnification, (c) 4YZ at high magnification, (d) 5YZ, (e) 6YZ at low magnification, and (f) 6YZ at high magnification. Low magnification images show the sporadic pores in 5YZ and 6YZ.

**Table 2**
$\frac{Y}{Zr}$ ratio at the grain surface of the YZ samples sintered at 1400 °C for 5 h. See text and Fig. 2 for the detail.

| Sample | $\frac{Y}{Zr}$ ratio |
|---|---|
| 3YZ | 0.18 ± 0.019 for large grains, 0.13 ± 0.002 for small grains |
| 4YZ | 0.13 ± 0.004 |
| 5YZ | 0.25 ± 0.009 for large grains; 0.15 ± 0.005 for small grains |
| 6YZ | 0.22 ± 0.004 for large grains; 0.13 ± 0.001 for small grains |

3YZ is consistent with the literature report [8,32], even with alumina dopant [45].

### 3.4. Translucency and gloss

The translucency parameter, $\Delta E_{2000}$, and the gloss unit of the YZ specimens are shown in Fig. 5. $\Delta E_{2000}$ increases from 2.37 to 2.74 with increase in $Y_2O_3$ content from 3 mol% to 5 mol%, followed by a decreased value of 1.35 for 6YZ. Translucency parameter values are consistent with the literature report of similar thickness [46]. The glossiness also increases up to 5 mol% $Y_2O_3$ and then decreases for 6 YZ. The measured translucency parameter is a combined effect of structure

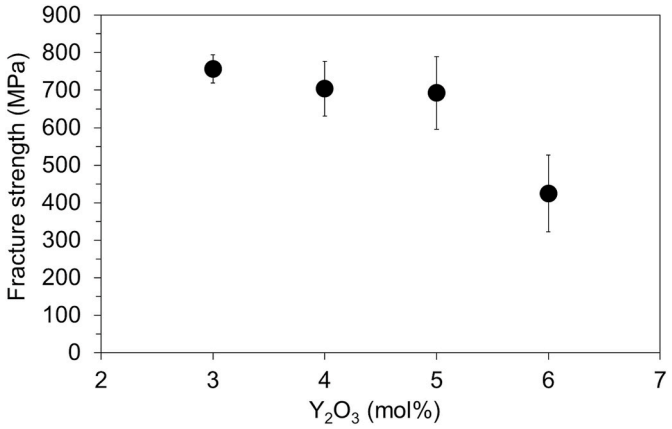


**Fig. 3.** Biaxial flexural strength of the YZ samples sintered at 1400 °C for 5 h.

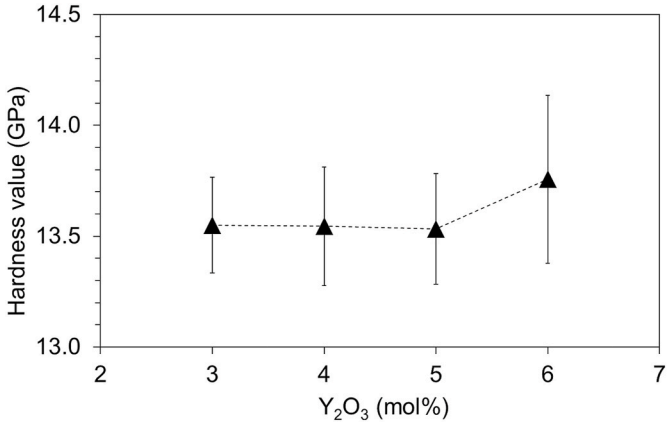


**Fig. 4.** Vickers micro-hardness of the YZ samples sintered at 1400 °C for 5 h.

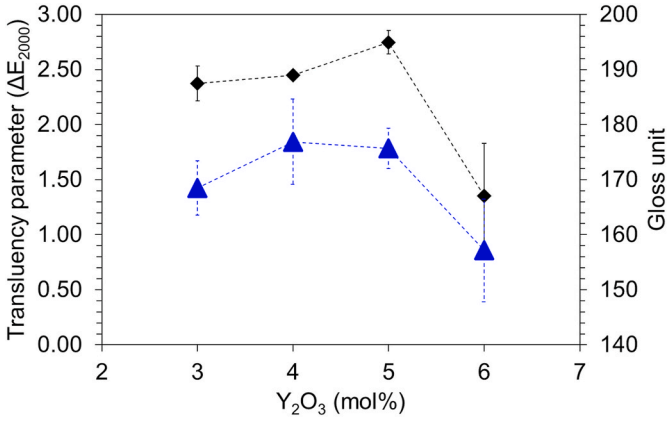


**Fig. 5.** Translucency parameter and gloss unit of the YZ samples sintered at 1400 °C for 5 h. Diamond shaped symbols indicate translucency parameter and the triangle symbols refer to gloss unit.

and microstructure of the studied YZ specimens. $Y_2O_3$ content decreases birefringence due to increasing cubic polymorph, and increases point defects (oxygen vacancies and cation vacancies) and porosities. Decreasing birefringence should increase translucency but point defects and pores scatter light [47–49]. $Y^{3+}$segregation at the surface also contributes to light scattering. Negligible $\frac{Y}{Zr}$ variation in different grains attributes to the highest translucency for 5YZ. Higher porosity and $\frac{Y}{Zr}$ variation among grains (surface segregation) account for the lowest translucency of 6YZ.

### 3.5. Low temperature degradation (LTD)

Low temperature degradation (LTD) of the YZ specimens are reported as monoclinic phase fraction (%) after aging of the YZ specimens in water at 134 °C. The XRD plots of the aged specimens are shown in Fig. 6 only for 5 h and 108 h for brevity. It is evident that the 6YZ is degradation resistant for 5 h aging time while other specimens degrade. As the aging time increases to 108 h, the intensity corresponding to the monoclinic phase increases and tetragonal phase decreases. Monoclinic phase is also observed for the 6YZ. These observations confirm that the extent of degradation increases with increase in aging time. According to a test protocol, although debatable, 5 h aging of YZ at 134 °C replicates 10–20 years in vivo (37 °C in human body) lifetime [50]. It is implied that 6YZ specimen which contains 60% cubic phase, as per the powder batch, is expected to remain stable for at least 10 years.

Fig. 7 shows the extent of LTD (% monoclinic) of the YZ specimens with aging time. $Y_2O_3$ dopant in $ZrO_2$ generates oxygen vacancies to maintain charge neutrality according to the Kroger-Vink notation

$$Y_2O_3 \xrightarrow{2ZrO_2} 2Y'_{Zr} + V_O^{\cdot\cdot} + 3O_O^{\times}$$

The oxygen vacancies reorganize the atomic arrangement in the crystal lattice to attain thermodynamic stability [51]. The thermodynamic stability of YZ increases with $Y_2O_3$ content [52,53] and cubic polymorph [51]. Accordingly, the LTD is the lowest for 6YZ.

The oxygen vacancies in YZ are annihilated by dissociative adsorption of $H_2O$ molecules according to

$$H_2O + V_O^{\cdot\cdot} + O_O^{\times} \leftrightarrow 2(OH)_O^{\cdot}$$

Oxygen vacancy annihilation precipitates the $Y^{3+}$ ions from the surface lattice, accompanied with lattice distortion, to maintain charge neutrality. Subsequently, $t \rightarrow m$ polymorphic transformation occurs. The repulsive force between $Y^{3+}$ cations and localized lattice distortion lead

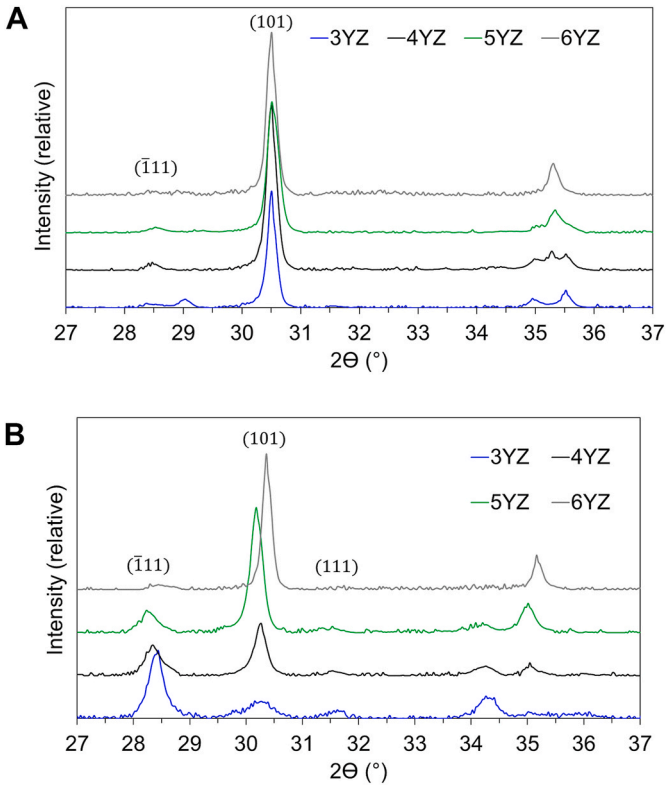


**Fig. 6.** XRD plots YZ samples aged in water at 134 °C for (a) 5 h and (b) 108 h.

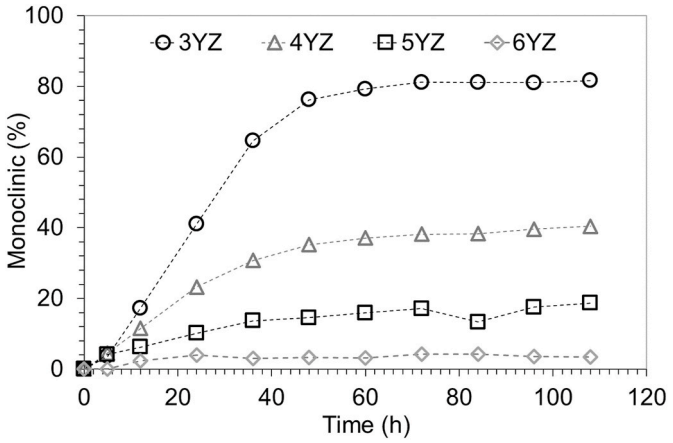


**Fig. 7.** Monoclinic phase percentage in the YZ samples aged in water at 134 °C for 5 h–108 h.

to surface segregation.

6YZ exhibits superior LTD resistance but inferior mechanical and optical properties while 5YZ exhibits a trade-off between these properties. Microstructural defects such as pores, and non-uniform grain size distribution due to grain growth during sintering attribute to the inferior mechanical and optical properties. These properties can significantly be improved in 6YZ by developing defect-free microstructure by optimized sintering kinetics.

## 4. Conclusions

Biaxial flexural strength, hardness, translucency and gloss, and low temperature degradation (LTD) of 3–6 mol% yttria stabilized zirconia (3-6YZ) have been investigated for the samples sintered at 1400 °C for 5 h. The density of the YZ samples decreases and the apparent porosity increases with increase in $Y_2O_3$ content. Uniform grains of (~0.33 μm) are found in 3YZ and 5YZ while non-uniform grain size distribution is observed for 4YZ and 6YZ. The Vickers microhardness and the biaxial flexural strength are, respectively, ~13.5 GPa and ~750 MPa for all the YZ samples except for 6YZ. Increasing $Y_2O_3$ decreases the birefringence effect and increases translucency, being the highest for 5YZ. Microstructural defects (pores, non-uniform grain size, and $Y^{3+}$ segregation at surface) contribute to the decrease in strength and translucency for 6YZ. LTD ($t \rightarrow m$ phase transformation) decreases with increase in $Y_2O_3$ content due to decreased tetragonality and abundance of oxygen vacancies for structural stability. Less than 5% monoclinic phase was detected for 6YZ but ~80% for 3YZ after aging in a hydrothermal autoclave at 134 °C for 108 h.

## Declaration of competing interest

The authors declare that they have no known competing financial interests or personal relationships that could have appeared to influence the work reported in this paper.

## Acknowledgement

S. R is grateful to the CORD UAB Summer Science Institute for providing the UAB Blazing to Biomedical Careers Program (BBC) internship.

## References

[1] Grand View Research, Dental Implants Market Size, Share & Trends Analysis Report by Product (Titanium Implants, Zirconium Implants), by Region (North America, Europe, Asia Pacific, Latin America, MEA), and Segment Forecasts, 2020, 2027, https://www.grandviewresearch.com/industry-analysis/dental-implants-market. (Accessed 27 November 2020).
[2] H.J. Wenz, J. Bartsch, S. Wolfart, M. Kern, Osseointegration and clinical success of zirconia dental implants: a systematic review, Int. J. Prosthodont. (IJP) 21 (2008) 27–36.
[3] S. Roehling, K.A. Schlegel, H. Woelfler, M. Gahlert, Zirconia compared to titanium dental implants in preclinical studies - a systematic review and meta-analysis, Clin. Oral Implants Res. 30 (2019) 365–395.
[4] T. Hanawa, Zirconia versus titanium in dentistry: a review, Dent. Mater. J. 39 (2020) 24–36.
[5] Center for Devices and Radiological Health Continued 2001, U.S. Food & Drug Administration. https://www.fda.gov/inspections-compliance-enforcement-and-criminal-investigations/enforcement-story-archive/center-devices-and-radiological-health-continued-2001 (accessed 27 November 2020).
[6] K. Haraguchi, N. Sugano, T. Nishii, H. Miki, K. Oka, H. Yoshikawa, Phase transformation of a zirconia ceramic head after total hip arthroplasty, J. Bone Joint Surg. Br. 83 (2001) 996–1000.
[7] J.L. Masonis, R.B. Bourne, M.D. Ries, R.W. McCalden, A. Salehi, D.C. Kelman, Zirconia femoral head fractures - a clinical and retrieval analysis, J. Arthroplasty 19 (2004) 898–905.
[8] C. Piconi, G. Maccauro, L. Pilloni, W. Burger, F. Muratori, H.G. Richter, On the fracture of a zirconia ball head, J. Mater. Sci. Mater. Med. 17 (2006) 289–300.
[9] M. Monzavi, S. Noumbissi, H. Nowzari, The impact of in vitro accelerated aging, approximating 30 and 60 years in vivo, on commercially available zirconia dental implants, Ciln. Implant Dent, Relat. Res. 19 (2017) 245–252.
[10] F. Zhang, H. Reveron, B.C. Spies, B.V. Meerbeek, J. Chevalier, Trade-off between fracture resistance and translucency of zirconia and lithium-disilicate glass ceramics for monolithic restorations, Acta Biomater. 91 (2019) 24–34.
[11] J. Chevalier, L. Gremillard, S. Deville, Low-temperature degradation of zirconia and implications for biomedical implants, Annu. Rev. Mater. Res. 37 (2007) 1–32.
[12] M.C. Aragón-Duartea, A. Nevarez-Rascónb, H.E. Esparza-Poncea, M.M. Nevarez-Rascónb, R.P. Talamantesa, C. Ornelasa, J. Mendez-Nonella, J. González-Hernándezc, M.J. Yacamánd, A. Hurtado-Macíasa, Nanomechanical properties of zirconia- yttria and alumina zirconia- yttria biomedical ceramics, subjected to low temperature aging, Ceram. Int. 43 (2017) 3931–3939.
[13] K.P. Kyrana, M. Fasoula, E. Kontonasaki, Translucency of monolithic zirconia after hydrothermal aging: a review of in vitro studies, J. Prosthodont. 29 (2020) 489–500.
[14] X. Guo, J. He, Hydrothermal degradation of cubic zirconia, Acta Mater. 51 (2003) 5123–5130.
[15] D. Kim, H. Jung, D. Cho, Phase transformations of $Y_2O_3$ and $Nb_2O_5$ doped tetragonal zirconia during low temperature aging in air, Solid State Ionics 80 (1995) 67–73.
[16] X. Guo, T. Schober, Water incorporation in tetragonal zirconia, J. Am. Ceram. Soc. 87 (2004) 746–748.
[17] P. Pandoleon, E. Kontonasaki, N. Kantiranis, N. Pliatsikas, P. Patsalas, L. Papadopoulou, T. Zorba, K.M. Paraskevopoulos, P. Koidis, Aging of 3Y-TZP dental zirconia and yttrium depletion, Dent. Mater. 33 (2017) e385–e392.
[18] A.E. Hughes, F.T. Ciacchi, S.P.S. Badwal, Role of $O^{2-}$, $OH^-$ and anion vacancies in the degradation of Y-TZP in moist environments, J. Mater. Chem. 4 (1994) 257–263.
[19] S. Ramesh, K.Y. Sara Lee, C.Y. Tan, A review on the hydrothermal ageing behaviour of Y-TZP ceramics, Ceram. Int. 44 (2018) 20620–20634.
[20] J. Chevalier, S. Deville, E. Münch, R. Jullian, F. Lair, Critical effect of cubic phase on aging in 3 mol% yttria-stabilized zirconia ceramics for hip replacement prosthesis, Biomaterials 25 (2004) 5539–5545.
[21] T.J. Lucas, N.C. Lawson, G.M. Janowski, J.O. Burgess, Effect of grain size on the monoclinic transformation, hardness, roughness, and modulus of aged partially stabilized zirconia, Dent. Mater. 31 (2015) 1487–1492.
[22] A. Suresh, M.J. Mayo, W.D. Porter, Thermodynamics of the tetragonal-to-monoclinic phase transformation in fine and nanocrystalline yttria-stabilized zirconia powders, J. Mater. Res. 18 (2003) 2912–2921.
[23] G. Sharma, S.V. Ushakov, A. Navrotsky, Size driven thermodynamic crossovers in phase stability in zirconia and hafnia, J. Am. Ceram. Soc. 101 (2018) 31–35.
[24] J.W. Drazin, R.H.R. Castro, Phase stability in nanocrystals: a predictive diagram for yttria–zirconia, J. Am. Ceram. Soc. 98 (2015) 1377–1384.
[25] H.G. Scott, Phase relationships in the zirconia - yttria system, J. Mater. Sci. 10 (1975) 1527–1535.
[26] F. Zhang, K. Vanmeensel, M. Batuk, J. Hadermann, M. Inokoshi, B.V. Meerbeek, I. Naert, J. Vleugels, Highly-translucent, strong and aging-resistant 3Y-TZP ceramics for dental restoration by grain boundary segregation, Acta Biomater. 16 (2015) 215–222.
[27] A.A. Nogiwa-Valdez, W.M. Rainforth, P. Zeng, I.M. Ross, Deceleration of hydrothermal degradation of 3Y-TZP by alumina and lanthana co-doping, Acta Biomater. 9 (2013) 6226–6235.
[28] F. Zhang, K. Vanmeensel, M. Inokoshi, M. Batuk, J. Hadermann, B. Van Meerbeek, I. Naert, J. Vleugels, Critical influence of alumina content on the low temperature degradation of 2–3 mol% yttria-stabilized TZP for dental restorations, J. Eur. Ceram. Soc. 35 (2015) 741–750.
[29] K. Matsui, K. Nakamura, A. Kumamoto, H. Yoshida, Y. Ikuhara, Low-temperature degradation in yttria-stabilized tetragonal zirconia polycrystal doped with small amounts of alumina: effect of grain-boundary energy, J. Eur. Ceram. Soc. 36 (2016) 155–162.
[30] I.G. Tredici, M. Sebastiani, F. Massimi, E. Bemporad, A. Resmini, G. Merlati, U. Anselmi-Tamburini, Low temperature degradation resistant nanostructured yttria-stabilized zirconia for dental applications, Ceram. Int. 42 (2016) 8190–8197.

[31] A. Harada, S. Shishido, S. Barkarmo, R. Inagaki, T. Kanno, U. Ortengren, H. Egusa, K. Nakamura, Mechanical and microstructural properties of ultra-translucent dental zirconia ceramic stabilized with 5 mol% yttria, J. Mech. Behav. Biomed. Mater. 111 (2020) 103974.
[32] F. Zhang, B.V. Meerbeek, J. Vleugels, Importance of tetragonal phase in high-translucent partially stabilized zirconia for dental restorations, Dent. Mater. 36 (2020) 491–500.
[33] C. dos Santos, G.O. Rosa, M.N. Quintino, M.F.R.P. Alves, S. Ribeiro, C.L. Melo-Silvad, Effect of surface finishing and thickness on the translucency of zirconia dental ceramics, Ceram. Int. 46 (2020) 7748–7755.
[34] Y. Hayaishi, H. Miki, H. Yoshikawa, N. Sugano, Phase transformation of a new generation yttria-stabilized zirconia femoral head after total hip arthroplasty, Mod. Rheumatol. 18 (2008) 647–650.
[35] S. Fabris, A.T. Paxton, M.W. Finnis, A stabilization mechanism of zirconia based on oxygen vacancies only, Acta Mater. 50 (2002) 5171–5178.
[36] J.F. Bartolomé, I. Montero, M. Díaz, S. López-Esteban, J.S. Moya, S. Deville, L. Gremillard, J. Chevalier, G. Fantozzi, Accelerated aging in 3-mol%-yttria-stabilized tetragonal zirconia ceramics sintered in reducing conditions, J. Am. Ceram. Soc. 87 (2004) 2282–2285.
[37] Standard Test Method for Water Absorption, Bulk Density, Apparent Porosity, and Apparent Specific Gravity of Fired Whiteware Products, 2006. ASTM C373 – 88.
[38] Dentistry - Ceramic Materials, ISO 6872:2015..
[39] Standard Test Method for Vickers Indentation Hardness of Advanced Ceramics, 2019. ASTM C1327 – 15.
[40] M.R. Luo, G. Cui, B. Rigg, The Development of the CIE 2000 colour-difference formula: CIEDE2000, Color Res. Appl. 26 (2001) 340–350.
[41] H. Toraya, M. Yoshimura, S. Shigeyuki, Calibration curve for quantitative analysis of the monoclinic-tetragonal $ZrO_2$ systems by X-ray diffraction, J. Am. Ceram. Soc. 67 (1984) C119–C121.
[42] M. Yashima, M. Kakihana, M. Yoshimura, Metastable-stable phase diagrams in the zirconia-containing systems utilized in solid-oxide fuel cell application, Solid State Ionics 86–88 (1996) 1131–1149.
[43] N.M. Moqbel, M. Al-Akhali, S. Wille, M. Kern, Influence of aging on biaxial flexural strength and hardness of translucent 3Y-TZP, Materials 13 (2020) 27, 2020.
[44] Z. Gong, W. Zhao, K. Guan, P. Rao, Q. Zeng, J. Liu, Z. Feng, Influence of grain boundary and grain size on the mechanical properties of polycrystalline ceramics: grain-scale simulations, J. Am. Ceram. Soc. 103 (2020) 5900–5913.
[45] F. Zhang, M. Inokoshi, M. Batuk, J. Hadermann, I. Naert, B.V. Meerbeek, J. Vleugels, Strength, toughness and aging stability of highly-translucent Y-TZP ceramics for dental restorations, Dent. Mater. 32 (2016) e327–e337.
[46] T. Nakamura, Y. Nakano, H. Usami, K. Wakabayashi, H. Ohnishi, T. Sekino, H. Yatani, Translucency and low-temperature degradation of silica-doped zirconia: a pilot study, Dent. Mater. J. 35 (2016) 571–577.
[47] J. Klimke, M. Trunec, A. Krell, Transparent tetragonal yttria-stabilized zirconia ceramics: influence of scattering caused by birefringence, J. Am. Ceram. Soc. 94 (2011) 1850–1858.
[48] A. Krell, J. Klimke, T. Hutzler, Transparent compact ceramics: inherent physical issues, Opt. Mater. 31 (2009) 1144–1150.
[49] I. Yamashita, K. Tsukuma, Light scattering by residual pores in transparent zirconia ceramics, J. Ceram. Soc. Japan 119 (2011) 133–135.
[50] C. Sanon, J. Chevalier J, T. Douillard, M. Cattani-Lorente, S.S. Scherrer, L. Gremillard, A new testing protocol for zirconia dental implants, Dent. Mater. 31 (2015) 15–25.
[51] S. Fabris, A.T. Paxton, M.W. Finnis, A stabilization mechanism of zirconia based on oxygen vacancies only, Acta Mater. 50 (2002) 5171–5178.
[52] G.C.C. Costa, S.V. Ushakov, R.H.R. Castro, A. Navrotsky, R. Muccillo, Calorimetric measurement of surface and interface enthalpies of yttria-stabilized zirconia (YSZ), Chem. Mater. 22 (2010) 2937–2945.
[53] J.W. Drazin, R.H.R. Castro, Phase stability in nanocrystals: a predictive diagram for yttria - zirconia, J. Am. Ceram. Soc. 98 (2015) 1377–1384.